Pergamon

Solid State Communications, Vol. 97, No. 12, pp. 1085–1089, 1996

0038–1098/96 $12.00+.00

0038–1098(95)00702-4

# PHASE TRANSITIONS AND "NONMETALLIC" TEMPERATURE DEPENDENCE OF CONDUCTION ELECTRON SPIN RESONANCE LINE WIDTH IN QUASI-TWO-DIMENSIONAL SYNTHETIC METAL $C_{15}HNO_3$

A.M. Ziatdinov and N.M. Mishchenko

Institute of Chemistry, Russian Academy of Sciences, 100-let Vladivostoku, 159, 690022 Vladivostok, Russia

(*Received* 10 *May* 1995; *accepted in revised form* 10 *October* 1995 *by P.H. Dederichs*)

In the synthetic metal $C_{15}HNO_3$ during and after crystallization of the $HNO_3$ "guest" molecules, the simultaneous increase of conductivity, conduction electron spin resonance (CESR) line width and spin carriers concentration ($N$) was found and investigated. The increase of $N$ is directly connected with the partial localization of the conduction $\pi$-electrons (in terms of graphite intercalation compounds tight binding model). Since the localized electrons are the perturbation centres for the conduction electrons, it has been proposed that the increase of their concentration is the main reason for the decrease of the in-plane spin carriers mobility and the "nonmetallic" increase of the CESR line width observed during and after crystallization of the $HNO_3$ "guest" layers.

Keywords: A. metals, D. electronic transport, D. phase transitions, E. electron paramagnetic resonance.

## 1. INTRODUCTION

THE TEMPERATURE dependence of the conduction electron spin resonance (CESR) line width ($\Delta B$) in metals has been successfully explained [1] in terms of the Elliot's theory [2] according to which $\Delta B = \alpha(\Delta g)^2/\tau$, where $\alpha$ is a constant, $\Delta g$ is the $g$-shift from the free electron value, and $\tau$ is the conductivity relaxation time. The frequency of the electron–electron and electron–phonon collisions decreases with temperature and, as a result, $\tau$ increases, while the concentration ($N$) of the current carriers remains practically constant because of large values of Fermi temperature [3]. As a result, when the temperature lowers, the conductivity of pure metals $\sigma = Ne^2\tau/m^* = Ne\mu$ ($m^*$, $e$ and $\mu$ are the effective mass, charge and mobility of charge carriers, respectively) increases, and simultaneously, if $\Delta g$ is temperature independent, the CESR line width decreases.

In graphite intercalation compounds (GICs) of the acceptor type $C_{15}HNO_3$ we found a relation between $\sigma$ and $\Delta B$ other than in pure metals. In this synthetic metal during and after intercalate crystallization $\Delta g$ is unchanged, while both the electroconductivity and the CESR line width increase simultaneously. In this paper we report the results of an investigation of the CESR line width "nonmetallic" temperature dependence origin in GIC $C_{15}HNO_3$.

## 2. EXPERIMENTAL

GICs comprise a wide class of synthetic metals and consist of an alternating sequence of $n$ hexagonal graphite monolayers ($n$ is the stage index) and a monolayer of "guest" atoms or molecules (intercalate) [4]. The compounds $C_{15}HNO_3$ investigated belong to the third stage of $\alpha$-modification of GICs with nitric acid of the general formula $C_{5n}HNO_3$ ($n = 1, 2, 3, \ldots$) [4, 5]. According to the data of various physical methods [4], in these GICs the two-dimensional liquid-like layers of $HNO_3$ are ordered and form a two-dimensional crystal at temperatures lower than $T \sim 250$ K. Layers of $HNO_3$ may be incommensurable with a carbon net along one of its crystallographic directions and they undergo a structural phase transition of the incommensurate phase–commensurate phase type at $T \sim 210$ K [6].

CESR spectra of GIC $C_{15}HNO_3$ plates were registered at X-band ($\nu = 9.52$ GHz) in the temperature range 100–300 K using the rectangular resonator with the $TE_{102}$ mode and 2.5 kHz modulation of an external constant magnetic field $\mathbf{B}_0$. At the conventional setting of the rectangular resonator, the electrical component of the microwave field is parallel to $\mathbf{B}_0$; in the geometric center of the resonator the magnetic component of the microwave field is parallel to the vertical axis of the resonator.

Highly oriented pyrolitic graphite plates required for GIC synthesis were cut out of a single bar with the basal plane conductivity equal to $(1.2 \pm 0.2) \times 10^4\,\mathrm{Ohm^{-1}\,cm^{-1}}$. These plates had a shape of a rectangular parallelepiped with dimensions: width ($l$) × height ($h$) × thickness ($d$), where $l \times h$ is the square of a basal plane. Accuracy in determining the size of plates was $\sim 5 \times 10^{-4}$ cm. Synthesis of GIC $C_{15}HNO_3$ was carried out in nitric acid with the density $\rho = 1.49\,\mathrm{g\,cm^{-3}}$. The GIC stage was controlled by the diffraction method. The effect of temperature on CESR line shape parameters was investigated using the plate of size $0.40 \times 0.40 \times 0.02\,\mathrm{cm^3}$.

## 3. RESULTS AND DISCUSSION

In the entire temperature range of investigations a single asymmetric CESR signal of $C_{15}HNO_3$ is observed. Down to ~247 K the asymmetry parameter of the first derivative of the absorption line $A/B$ (which is defined as the ratio of the maximum peak height ($A$) to the minimum peak height ($B$), both measured with respect to the zero line of the resonance derivative) and the width of the CESR line at half height of the peak $A$ are independent of temperature and are equal to $3.3 \pm 0.1$ and $6.0 \times 10^{-5}$ T, respectively. At all temperatures, the spectrum is axial with respect to the **c**-axis and is characterized by $g_\parallel = 2.0023 \pm 0.0001$ and $g_\perp = 2.0028 \pm 0.0001$. The line width increases as temperature decreases below than 247 K (Figs 1 and 2). Simultaneously, the $A/B$ value decreases, and it is equal to $2.9 \pm 0.1$ at 110 K (Fig. 2). The derivative $\mathrm{d}(\Delta B)/\mathrm{d}T$ has peaks at $T_{c1} \simeq 244$ K, $T_{c2} \simeq 242$ K and $T_{c3} \simeq 212$ K (Figs 1 and 2). As the temperature increases, $\Delta B$ and $A/B$ values change inversely but with a "global" temperature hysteresis (Figs 1 and 2). Temperatures $T_{c1}^-$ ($T_{c1}^+$) and $T_{c2}^-$ ($T_{c2}^+$) are close to the temperature of the intercalate crystallization (melting) in $C_{15}HNO_3$ ($T_c \sim 250$ K) known from literature [4]. This allows us to treat the CESR line shape transformations observed in $C_{15}HNO_3$ at $T_{c1}^-$ ($T_{c1}^+$) and $T_{c2}^-$ ($T_{c2}^+$) as a result of the two-step change in the aggregate state of the "guest" molecules. The CESR line shape transformation at $T_{c3}$, is probably due to the incommensurate–commensurate phase transition. At powers of the microwave field far from saturation of the CESR signal and at the same temperature, $\Delta B$ values in $Q$- and $X$-bands coincide indicating that the CESR line is homogeneously broadened.

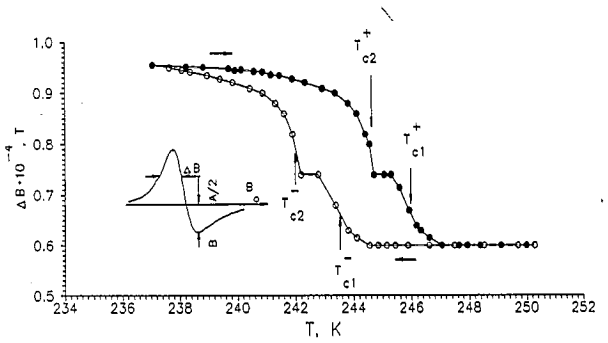


Fig. 1. Temperature dependence of CESR linewidth $\Delta B$ of $C_{15}HNO_3$ plate with dimensions: $0.4 \times 0.4 \times 0.02\,\mathrm{cm^3}$ during crystallization (unfilled symbols) and melting (filled symbols) of intercalate. $T_{c1}^-$ ($T_{c1}^+$) and $T_{c2}^-$ ($T_{c2}^+$) are the temperatures of the first and second peaks of the derivative $\mathrm{d}(\Delta B)/\mathrm{d}T$ at cooling (heating) of the sample, respectively. $\mathbf{B}_0 \perp \mathbf{c}$, $\nu = 9.52$ GHz.

The basal plane electroconductivity ($\sigma_a$) of $C_{15}HNO_3$ plates was measured by the contactless induction method using a device analogous to that

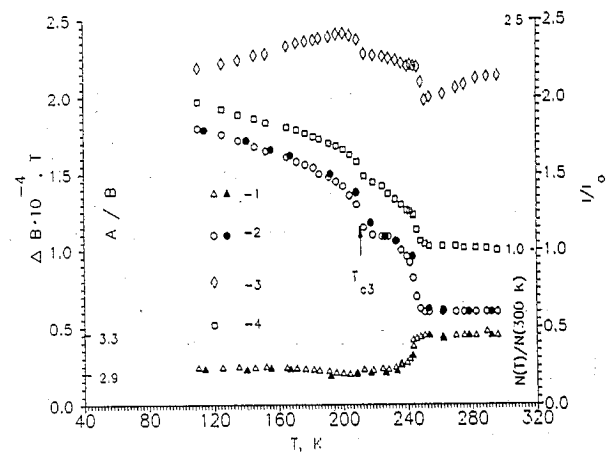


Fig. 2. Temperature dependence of CESR line parameters of $C_{15}HNO_3$ plate with dimensions: $0.4 \times 0.4 \times 0.02\,\mathrm{cm^3}$, i.e., $A/B(T)$ (curve 1), $\Delta B(T)$ (curve 2), $I(T)/I_0$ (curve 3), where $I = (A + B)\Delta B^2$ and $I_0$ is the intensity of the $Mn^{2+}$ ESR line in a standard sample $ZnS:Mn^{2+}$, and the relative spin concentration $N(T)/N(300\,\mathrm{K})$ (curve 4), determined by the expression (1). Unfilled (filled) symbols correspond to experimental values of parameters at cooling (heating) of the GIC. $T_{c3}$ is the temperature of the third peak of the derivative $\mathrm{d}(\Delta B)/\mathrm{d}T$. $\mathbf{B}_0 \perp \mathbf{c}$, $\nu = 9.52$ GHz.

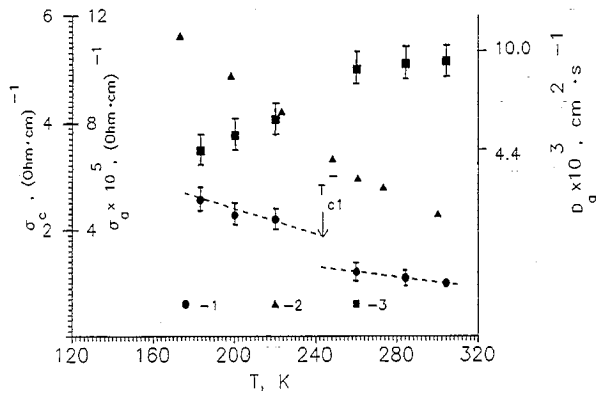


Fig. 3. Temperature dependence of $\sigma_c(1)$, $\sigma_a(2)$ and $D_a(3)$ in $C_{15}HNO_3$. The dashed line corresponds to the linear function $\sigma_c = [(-4.77 \times 10^{-3}\,K^{-1})\ T + 2.45]\ (\Omega\,cm)^{-1}$ and $\sigma_c = [(-1.76 \times 10^{-2}\,K^{-1})\ T + 5.79]\ (\Omega\,cm)^{-1}$ for $T > T_{c1}^-$ and $T < T_{c1}^-$, respectively.

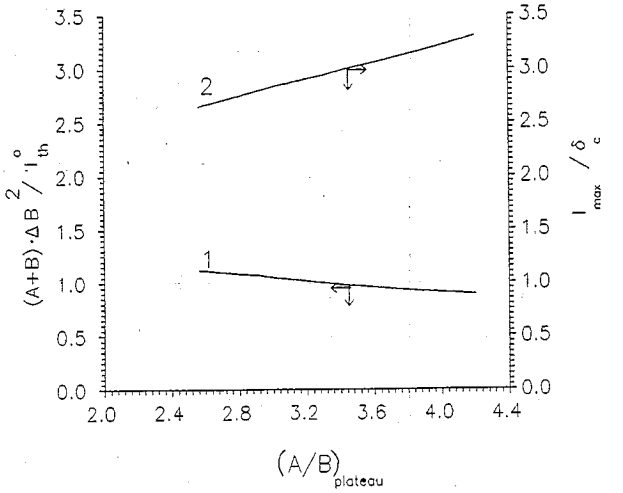


Fig. 4. The relation of theoretical value of intensity $(A+B)\Delta B^2/I_{th}^0$ (curve 1) and coordinate of the maximum $(l_{max}/\delta_c)$ of the theoretical dependence $A/B(l/\delta_c)$ (curve 2) plotted against the value of $A/B$ on the "plateau" of the $A/B(l/\delta)$ dependence (at $l/\delta_c > 10$). $I_{th}^0$ is the value of the $I_{th}$ at $A/B = 3.3$ (in quasi-liquid phase of the intercalate).

described by Pendrys *et al.* [7]. The results of $\sigma_a$ measurements are presented in Fig. 3, and indicate that the $\sigma_a$ increases as temperature decreases.

In the microwave field of a given configuration only the conduction plate regions adjacent to the vertical faces $(h \times l)$ and $(h \times d)$, situated approximately within the skin-depth, contribute to the CESR [8, 9]. In $C_{15}HNO_3$ one may neglect the contribution to CESR from regions adjacent to the basal planes $(h \times l)$ due to the high conduction anisotropy $(\sim 10^5)$ [4]. This peculiarity of $C_{15}HNO_3$ plates allows us to analyze their CESR line shape, in particular, at contactless determination of the **c**-axis electroconductivity $(\sigma_c)$ (see below), using the one-dimensional Dyson expression [10] for CESR line shape in isotropic metals and well known Feher and Kip [11] or Kodera [12] nomograms calculated on the basis of this expression.

The $\sigma_c$ measurement is not a trivial problem. The contactless method to determine the $\sigma_c$ of acceptor GICs was suggested by Saint-Jean and McRae [13]. They recommended the use of the well-known $A/B$ vs $l/\delta_c$ nomograms [8, 9, 12, 13] at interval $l/\delta_c < 2.5$ for this purpose. At this interval the ratio of $A/B$ does not depend on spin carrier mobility [8, 9, 12, 13]. This enables one to determine the value of $\delta_c$ and, consequently, the value of $\sigma_c$ unambiguously, by measuring the values of $A/B$ and $l$. However, in narrow samples of GICs with $HNO_3$ [14] as well as in narrow samples of GICs with $AsF_5$ [13] the values of $\sigma_c$ and spin carrier diffusion constant differ from values of this parameter in wide samples. This unusual result for narrow GIC samples is likely connected with the fact that the intercalate layers' composition and organization depend on a sample size [14]. That is why another contactless method was used to determine the value of $\sigma_c$ in our study. The principles of this method are as follows.

It follows from the one-dimensional Dyson expression for CESR line shape in metals [10] that the coordinate of the maximum $(l_{max}/\delta_c)$ of the $A/B(l/\delta_c)$ dependence and the value of asymmetry parameter on "plateau" (at $l/\delta_c > 10$) of this dependence $[(A/B)_{plat}]$ are unambiguously related to each other. The corresponding nomogram calculated by authors is presented in Fig. 4. The theoretical value of $l_{max}/\delta_c$ can be found from this nomogram, if the experimental value of $(A/B)_{plat}$ is known. Then, at a given frequency of the microwave field, the value of $\sigma_c$ can be easily calculated, if the experimental value of $l_{max}$ is known as well. It must be emphasized that the given procedure of $\sigma_c$-determination is applicable only in the case when (1) one may neglect the contribution to CESR from regions adjacent to the basal planes $(h \times l)$ of GIC plates and (2) the CESR line shapes of plates with $l \simeq l_{max}$ as well as plates with $l$ from "plateau" of the $A/B(l)$ dependence should be described by the one-dimensional Dyson expression for CESR line shape [10] with the same value of $\sigma_c$ and $T_{Da}$. Because of this, before the procedure under consideration was applied to determine the $\sigma_c$-value in $C_{15}HNO_3$, the experimental $A/B(l)$ dependence was studied in more detail at fixed temperature both before (at ~300 K) and after (at 220 and 183 K) the phase transition. Then this dependence was approximated by the corresponding theoretical curve calculated from the one-dimensional Dyson expression for CESR line shape [10] with the value of $\sigma_c$ determined

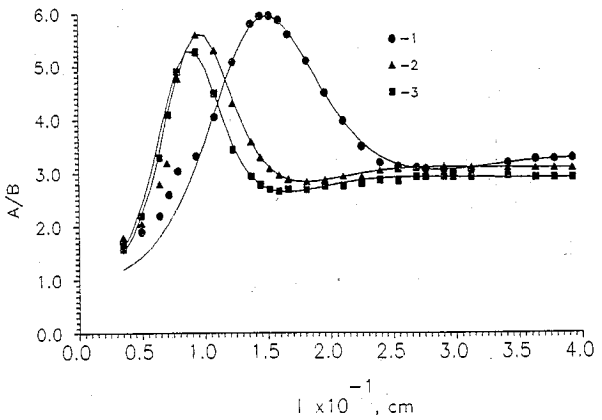


Fig. 5. The experimental (filled symbols) and theoretical (solid lines) values of the line asymmetry parameter $A/B$ of the $C_{15}HNO_3$ plates with dimensions $l \times 0.4 \times 0.02\,cm^3$ as a function of sample width ($l$). The experimental curves 1, 2 and 3 correspond to 300, 220 and 183 K, respectively. $\mathbf{B}_0 \perp \mathbf{c}$, $\nu = 9.52$ GHz. The theoretical curves at 300, 220 and 183 K are one-dimensional Dyson's [10] curves with $\sigma_c = 1.0$, 2.32 and $2.57\,\Omega^{-1}\,cm^{-1}$, $T_{Da} = 13.1$, 11.0 and 11.5, in the units of $10^{-8}$ s, respectively.

from the experimental values of $l_{max}$ and $(A/B)_{plat}$ and the value of $T_{Da}$ determined by the standard procedure [11, 12] (using the values of $\Delta B$ and $A/B$ of GIC plates with $l$ from "plateau" of the $A/B(l)$ dependence). As seen from Fig. 5, the theoretical and experimental dependences $A/B(l)$ are in good agreement at $l > l_{max}$. Taking it into consideration, the values of $\sigma_c$ at other temperatures were determined using the experimental values of $l_{max}$ and $(A/B)_{plat}$ only. By this procedure of $\sigma_c$-determination we established that $\sigma_c$, as well as $\sigma_a$ increases with decreasing the temperature (Fig. 3). Hence in $C_{15}HNO_3$, during and after intercalate crystallization the $\Delta B$ increases simultaneously with the conductivity in spite of the fact that the $g$-tensor values of the spin carriers are temperature independent. We have found a possible explanation for this uncommon property of the CESR line width temperature dependence by investigating the temperature effect on $N$ and on the in-plane spin diffusion constant ($D_a$).

At a given geometry of the GIC sample the CESR signal integral intensity $I = (A + B)\Delta B^2$ is proportional to $N\delta_c$. Because of this, the increase in $I$ simultaneously with the decrease in $\delta_c$, which takes place in $C_{15}HNO_3$ as the temperature decreases from $T_{c1}^-$ to $T_{c3}$ (Fig. 2), suggests that $N$ increases at this temperature range. This conclusion does not change once the 6.7% increase of $I$ (relative to its value in liquid phase of intercalate) along with the decrease of $A/B$ at this temperature range has been taken into consideration with the help of the corresponding nomogram in Fig. 4. Further, using the relation $I \sim N\delta_c$ and approximating the experimental values of $\sigma_c$ before and after phase transition by the linear function $[(-4.77 \times 10^{-3}\,K^{-1})\,T + 2.45]\,(\Omega\,cm)^{-1}$ and $[(-1.76 \times 10^{-2}\,K^{-1})\,T + 5.79]\,(\Omega\,cm)^{-1}$, respectively, we have calculated the temperature dependence of the relative spin carrier concentration (Fig. 2):

$$N(T)/N(300\,K) = [I(T)/I(300\,K] \times [\sigma_c(T)/\sigma_c(300\,K)]^{1/2}, \quad (1)$$

where $N(300\,K)$, $I(300\,K)$ and $\sigma_c(300\,K)$ are the values of $N$, $I$ and $\sigma_c$ at 300 K, respectively. As should be expected from the results of the qualitative analysis of the experimental data, $N$ increases as the temperature is lowered in the crystal phase of the intercalate (Fig. 2). Concerning the behaviour of $N$ in the quasi-liquid phase of the intercalate, all its variations occur within the experimental error (Fig. 2). It follows from above that in synthetic metal $C_{15}HNO_3$ in the solid phase of the intercalate the increase of $\sigma_a$ is at least partially due to the increase in $N$.

With knowledge of the experimental values of $A/B$ and $\Delta B$ of GIC plates with $l$ from "plateau" of the $A/B(l)$ dependence and using the Feher and Kip [11] nomograms one can easily determine the in-plane diffusion time across the skin-depth $\delta_c$ ($T_{Da}$) determined by the $\sigma_c$. According to Dyson [10], in approximation of independent electrons, the value of $T_{Da}$ is connected with the value of $D_a$ by the relationship $D_a = \delta_c^2/2T_{D_a}$. The estimation of $D_a$ according to these expressions has shown (Fig. 3) that its value during and after intercalate crystallization decreases.

The diffusion constant is equal to

$$D_a = \tfrac{1}{3}\Lambda_a v_a = \tfrac{1}{3}\tau_a v_a^2 \quad (2)$$

by definition [3]. In the expression (2) $\Lambda_a$, $\tau_a$ and $v_a$ are the mean free path, the electroconductivity relaxation time and the spin carriers velocity, all along the basal plane. If in expression (2) $v_a$ is identified with Fermi velocity $v_F$ and it is taken into account that in metals $v_F$ is proportional to the square of current carriers concentration [3] then it may be concluded, from this expression, that $\tau_a$ in $C_{15}HNO_3$ decreases during and after intercalate crystallization (since at this process $D_a$ decreases simultaneously with the increase of $N$). This suggests that "nonmetallic" broadening of the CESR line in $C_{15}HNO_3$ is due to the decrease of the in-plane current carriers mobility.

The broadening of the CESR line is homogeneous. The $g$-tensor values of spin carriers are independent of the changes in aggregate states of the intercalate and they are close to the $g$-tensor value of the free electron. These facts testify that the density of charge carriers

on intercalate molecules is small and does not change at phase transition. Above, it is shown that it is possible to analyze the transformations of the electronic properties of $C_{15}HNO_3$ induced by phase transition in terms of the rigid electronic band model of GICs [4, 15]. In terms of this model, in acceptor GICs related to the conductors with the hole Fermi surface [4] the increase of $N$ as the temperature decreases is possible only at lowering of the Fermi energy, for instance, due to the transfer of the additional electrons from carbon layers to intercalate layers [4, 15], or due to the localization of spin carriers in graphite layers, preferentially at the edges of the Dumas–Herold islands [16]. In this case, the increase in $N$ must obviously be accompanied by the decrease in $\tau_a$, and consequently, by the increase in $\Delta B$, because the localized electrons are the perturbation centers for the conduction electrons. That is, in the crystal phase of the "guest" molecules subsystem, the rigid electronic band model predicts qualitatively the correct temperature effect on these experimental values. Note that several recent experimental results confirm the existence in GICs of the localized moments and traps. For instance, Davidov *et al.* [17] observed the presence of localized moments in the graphite layers by spin–echo techniques performed on $AsF_5$ GICs and suggested the existence of traps. A precise analysis of the spin-relaxation time [13] and the anisotropy of the line width with the orientation of $\mathbf{B}_0$ [18] confirms this assumption. At the present time, the exact nature of this trap remains to be determined.

*Acknowledgements* — The authors are grateful to L.B. Nepomnyashchii (State Research Institute of Graphite, Moscow) for the HOPG plates used in the synthesis of GIC.

## REFERENCES

1. Monod P. & F. Beuneu, *Phys. Rev.* **B19,** 911 (1979).
2. R.J. Elliot, *Phys. Rev.* **96,** 266 (1954).
3. N.W. Ashcroft & D. Mermin, *Solid State Physics.* Cornel University, Holt, Rinehard and Winston, New York (1976).
4. M.S. Dresselhaus & G. Dresselhaus, *Adv. Phys.* **30,** 139 (1981).
5. M.J. Bottomly, G.S. Parry & A.R. Ubbelohde, *Proc. R. Soc. London* **A279,** 291 (1964).
6. F. Batallan, I. Rosenman, A. Maargl & H. Fuzellier, *Phys. Rev.* **B32,** 4810 (1985).
7. L.A. Pendrys, C. Zeller & F.L. Vogel, *J. Mat. Sci.* **15,** 2103 (1980).
8. A.M. Ziatdinov & N.M. Mishchenko, *Fiz. Tverd. Tela (Russia)* **36,** 8360 (1994).
9. J. Blinowski, P. Kacman, C. Rigaux & M. Saint-Jean, *Synth. Met.* **12,** 419 (1985).
10. F.J. Dyson, *Phys. Rev.* **98,** 349 (1955).
11. G. Feher & A.F. Kip, *Phys. Rev.* **98,** 337 (1955).
12. H. Kodera, *J. Phys. Soc. Jpn* **28,** 89 (1970).
13. M. Saint-Jean & E. McRae, *Phys. Rev.* **43,** 3969 (1991).
14. A.M. Ziatdinov & N.M. Mishchenko, Unpublished data.
15. S.Y. Leung & G. Dresselhaus, *Phys. Rev.* **B24,** 3490 (1981).
16. A.M. Ziatdinov, N.M. Mishchenko & Yu.M. Nikolenko, *Synth. Met.* **59,** 253 (1993).
17. D. Davidov, A. Grupp, H. Kass & P. Hoffer, *Synth. Met.* **23,** 291 (1988).
18. S. Shimamura, *Synth. Met.* **12,** 365 (1985).